Robust Detection and Mitigation of Mutual Interference in Automotive Radar

Christoph Fischer[*1], Hans Ludwig Blöcher[**], Jürgen Dickmann[**], Wolfgang Menzel[***]

[*]now with Airbus Defence and Space GmbH
Wörthstr. 85, 89077 Ulm, Germany
Email: christoph.c.fischer@airbus.com

[**]Daimler AG, Environment Perception
Wilhelm-Runge-Str. 11, 89081 Ulm, Germany

[***]Institute of Microwave Techniques, University of Ulm
Albert-Einstein-Allee 41, 89069 Ulm, Germany

Abstract: *Active safety functions are being integrated into more and more cars. Many of these rely on radar sensors as a source of information about surrounding objects. Based on this information, for example, emergency braking maneuvers are initiated. This requires a very high reliability of the provided data. In the long term, these requirements will become even stricter as highly automated driving comes into play. In the near future, this will result in a high density of radar sensors operating simultaneously and in close proximity. This constellation generates mutual car-to-car interference if no precautions are taken. At present, efforts in measures to mitigate the interference concentrate on time-frequency signal processing. Spatial filtering using digital beamforming is another powerful method. This paper aims to cover the chain of interference, from the basic principles of waveform interaction in a radar sensor's receiver stage, up to mitigation techniques and consequences for signal processing in the presence of interference.*

1. Introduction

Active safety systems are becoming standard equipment in more and more vehicles. These systems rely on accurate information about the environment around the vehicle. This information is acquired using a whole suite of sensors. Radar sensors have an important share of this sensor suite. They have the advantage of being quite independent of weather influence and external illumination. Additionally, radar sensors have the ability to measure relative velocities directly based on the Doppler effect. However, due to their active illumination, different radar sensors operating in the same frequency band may influence each other through their emissions. This issue has started to become of interest with the increasing market penetration of automotive radars and has been addressed in publicly funded projects like MOSARIM (More SAfety for everyone by Radar Interference Mitigation, [1]). One result of this project was that radar sensor design has to be aware of the different possible effects of mutual interference from the very beginning of the sensor development process. Taking this into account the issue of mutual interference is manageable. In this paper, the different aspects of FMCW interference from mechanisms to mitigation shall be covered.

2. Principles of FMCW radar and digital beamforming

For automotive radar at 77 GHz, FMCW [2] is one of the most widespread waveforms. Sensors employing this waveform transmit a frequency ramp with slope S and use the transmitted signal as the local oscillator signal for down converting the received signal (see

[1] The research leading to the presented results has been conducted by the author during his employment at Daimler AG in cooperation with the Institute of Microwave Techniques, University of Ulm.

the block diagram in Fig. 1). This results in a baseband signal with a greatly reduced bandwidth compared to the occupied RF bandwidth. For a target passing the observing sensor in a distance r under an angle α, the component $v \cdot \cos\alpha$ contributes to a Doppler frequency shift. The frequency of the baseband signal is

$$f_b(r,v) = f(v) + f(r) = f_0 \frac{2v}{c} \cos\alpha + S\frac{2r}{c} \quad (1)$$

The individual contributions from range and velocity cannot be resolved using a single measurement, but this so-called range-Doppler ambiguity can be solved in two different ways. One approach is, to transmit a sequence of fast ramps. The ramp duration is chosen such that the Doppler shift is negligible compared to the frequency shift produced by the range information of a target. Over the whole sequence of ramps the Doppler information can be obtained by evaluating the phase information of each range gate. From a signal processing point of view, the range and the Doppler processing are frequency analyses that can be jointly implemented employing a two dimensional FFT (Fast Fourier Transform).

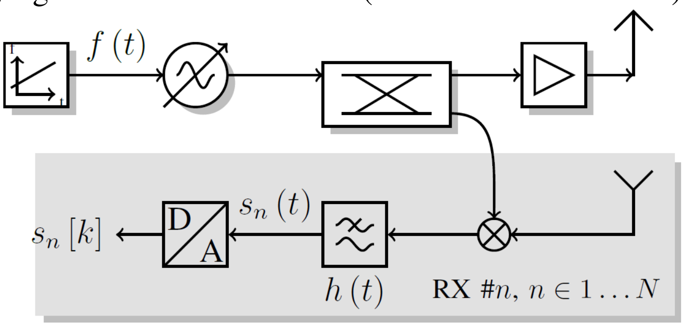

Figure 1: Basic block diagram of an FMCW radar sensor with signal generation and receiver stage. The receiver block (underlayed in gray) can be present N times resulting in N receive signals.

In the system considered here, digital beamforming (DBF) is used to acquire the angular position of a target. The sensor uses one transmit antenna with a large field of view to illuminate the scene. Multiple receivers with antennas at different positions result in N digitized baseband signals $s_n[k]$ (see Fig. 1). These digital signals can then be processed with the classical delay and sum or Bartlett beam former [3] that takes the signal vector $\boldsymbol{s}[k]$ and equalizes the phase differences φ between the channels (i.e. the individual components of the vector). This phase difference results from the incident angle of the impinging plane wave. The algorithm can also be reformulated in a way that it can be computed using another FFT. Consequently, when the chirp sequence waveform is utilized, raw signal processing in a digital beamforming radar can be implemented by three subsequent FFTs. These can be computed very efficiently by current digital signal processors (DSPs).
For improvement of angular resolution (and in principle also for the other FFT-based processing steps), an autoregressive filter can be used to compute additional, virtual antenna elements from the physically present receive channels [4]. The new, virtual antenna array can be processed like a physical array with this increased number of receive elements.

3. Mechanisms of FMCW and Chirp Sequence Interference

As introduced in the previous chapter, an FMCW type radar sensor uses the currently transmitted signal to down convert the received signal into the baseband. In case of another radar operating in the vicinity (the interferer, with an exemplary time dependent transmit frequency shown in Fig. 2), the transmission of this sensor will be down converted by the victim sensor (the sensor experiencing interference) just like a useful target return signal. As shown in [5-7] for mutual FMCW and in [8] for FMCW against chirp sequence interference, the resulting signal can be described by

$$s_{I,m}(m) = h(t) * \cos\left(\pi \Delta S t^2 + 2\pi f_{0,m} t + \varphi\right), \quad (2)$$

$$\Delta S = S_V - S_I \text{ and } f_{0,m} = f_{0,V} - f_{0,I} - mTS_I$$

with the victim's slope S_V, carrier frequency $f_{0,V}$, ramp duration T and ramp index m, the interferer's respective parameters indexed I, the low-pass filter impulse response $h(t)$, and an arbitrary phase term φ. Because of the low pass filter's small bandwidth relative to the overall bandwidth, the signal has a very short duration (cf. Fig. 2). When transformed into the range and Doppler domain, this short time domain signal generally has a broad bandwidth. When two identical radars interfere, there is also a probability of two parallel ramps occurring, so that a ghost target could appear. This probability for two parallel ramps is given in [9] by

$$P_{FT} = \frac{2B_{IF}}{B_{RF}} \cdot \frac{T}{T+T_D}, \tag{3}$$

with the RF and IF bandwidths B_{RF} and B_{IF}, the ramp time T, and the delay between subsequent ramps T_D. However, this probability does not consider the coherency of the two radar sensors. So even if two parallel ramps occur at the right time, a ghost target will most likely resemble a broad noise increase centered on a certain frequency, as observed in [9], rather than a sharp peak. This is a result of the non-coherent local oscillators of two different radar sensors.

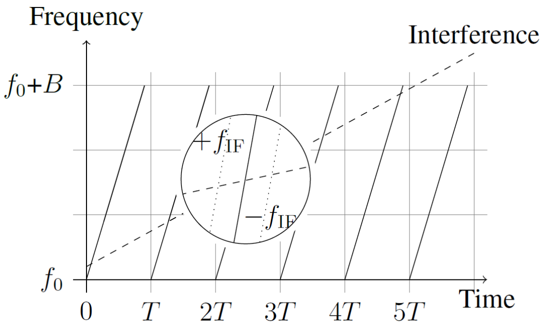

Figure 2: Graph showing the time dependent frequencies of a transmitted chirp sequence signal along with one FMCW interferer. Intersections in the spectrum at different frequencies are present for all but the last ramp. The inset is a magnified sketch of a ramp crossing with the IF bandwidth between $-f_{IF}$ and $+f_{IF}$.

4. Detection of Interference

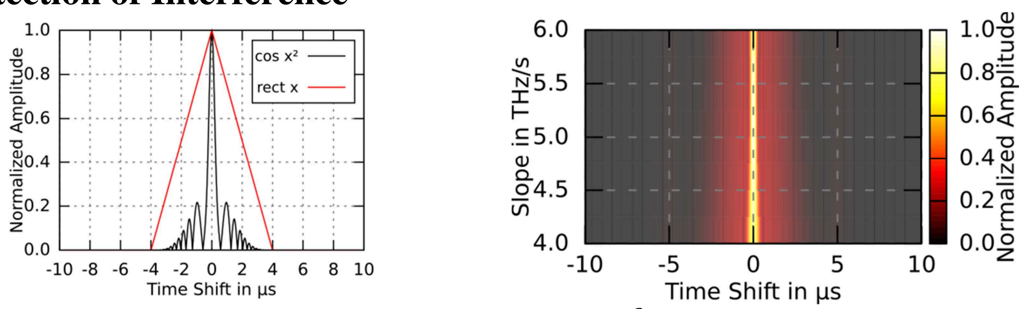

Figure 3: Evaluated autocorrelation functions of rect x and cos x^2, with an assumed slope of 5 THz/s and a resulting signal duration of 4 µs (left) and cross correlation function of a matched filter designed for a slope of 5 THz/s , an IF bandwidth of 10MHz and test signals with a relative slope ranging from 4 THz/s to 6 THz/s (right).

The detection of an interference signal can be performed in different ways. In this work, the energy detector and the matched filter will be investigated. The energy detector takes the sampled input signal $s[k]$ and computes the energy over a shorter sequence of this signal with length M, where M is the expected length of the interference signal. In order to exploit the knowledge that the interference signal has the structure given in (2) and further increase detection performance, a matched filter can be utilized. The respective autocorrelation functions of the energy detector and the matched filter are shown in Fig. 3 (left). The better performance of the matched filter can be seen from the sharper peak of the autocorrelation function. As the matched filter only fits one specific parameterization of (2) exactly, the correlation properties to a bandwidth of typical slopes are given in Fig. 3 (right). From the

numbers given in [10], an expected relative slope of 5±0.5 THz/s results for a typical chirp sequence sensor interfered by a slow FMCW sensor. It can be seen that the width of the correlation peak is almost constant over the whole band with a slight width increase at the edges of the investigated bandwidth.
After applying the matched filter or the energy detector, the detection of the interference can be performed by setting a threshold to the resulting correlation function. This can either be done with a fixed value or by computing an adaptive threshold using CFAR (Constant False Alarm Rate) techniques [11]. Detection in the measurement section of this paper has been performed using an OS-CFAR detector.

5. Interference Mitigation

When an interference signal has been detected, one option is to leave the signal untouched and set a flag that this measurement may be influenced by interference. Further signal processing like tracking can then consider the targets that have been observed in the measurement with less confidence than in an undisturbed measurement. The other choice is to suppress the interference signal. The decision whether to suppress the interference or to leave the received signal untouched depends on the maximum number of affected samples inside one single ramp $N_{I,s}$, the number of affected ramps $N_{I,l}$ and the maximum amplitude of the interference signal $A_{I,max}$. With these parameters, the maximum amplitude of a possibly resulting false point target is

$$A_{FT,max} \leq N_{I,s} \cdot N_{I,l} \cdot A_{I,max} \cdot C, \tag{5}$$

with the normalization constant C depending on the implementation of the time-frequency transformation. If this amplitude lies below the noise floor, no false target can arise from the interference signal and there is no need to use processing power to address this interference signal. Otherwise interference mitigation methods may be applied.
The simplest method is to set all samples affected by interference to zero. The drawback of this algorithm is that the detected peaks become broader in range and velocity domain because of the step introduced in the time domain signal. For better performance a window function can be applied to smoothen the edges and thereby reducing the widening of the detected peaks in range and Doppler [12]. The width in samples of the interference in one ramp $N_{I,s}$ and therefore the needed length of the zero sequence can be estimated by the expected minimum slope of the interference relative to the own sensor's slope S_{min}, the sampling frequency f_s and the IF bandwidth B_{IF}

$$N_{I,s} = \left\lceil \frac{\Delta S}{f_s B_{IF}} \right\rceil. \tag{6}$$

The used roll-off function can be selected from the known window functions depending on the desired performance parameters. The loss in SNR that is introduced by the weighting function w with length N can be computed by

$$L_0 = \frac{(\sum_n w_n)^2}{N \sum w_n^2}. \tag{7}$$

A sensor with multiple receive channels, has the possibility to use the spatial information to suppress the interference [13, 14]. Using the information from the detection step, the strongest signal in the affected samples is (with very high probability) the interfering one. Therefore this signal can be taken to compute a beam steering vector that has a null in the direction of this signal. This leaves the targets in other directions unaffected, i.e. no broadening of peaks in range or velocity domain occurs. The algorithm of the adaptive beamforming approach is straight forward. The samples identified by the interference detection step are used to compute new beamforming weights w_n for each channel n based on the strongest signal present in the interfered samples. The weights are chosen such that the strongest signal is suppressed in the output. In order to ensure numerical stability of the algorithm and to limit the suppression on the strongest signal, Diagonal Loading [16] is applied.

6. Measurement Setup and Results

The implemented measurement setup consists of an experimental, chirp sequence based radar sensor with 10 receive channels and one transmitter in the 76 GHz band, and the transmit bandwidth can be adjusted between zero and more than 1 GHz. The sampled and AD-converted time domain data of each receiver are transferred to a desktop PC and stored for further processing. The interferer used for the measurements was an unmodified medium-size car equipped with an adaptive cruise control (ACC) system that utilizes a radar sensor known to operate in the 76 GHz band. During the measurements the car approached the victim sensor from straight ahead; therefore the interference is expected from an angle of 0°. Signal processing is performed off-line using the FFT-based algorithms introduced in Section 2. To improve the angular resolution of the sensor, an autoregressive filter with five coefficients has been applied to extend the virtual aperture by a factor of three. Suppression of the interference has been added as an additional processing step before range and velocity FFT processing.

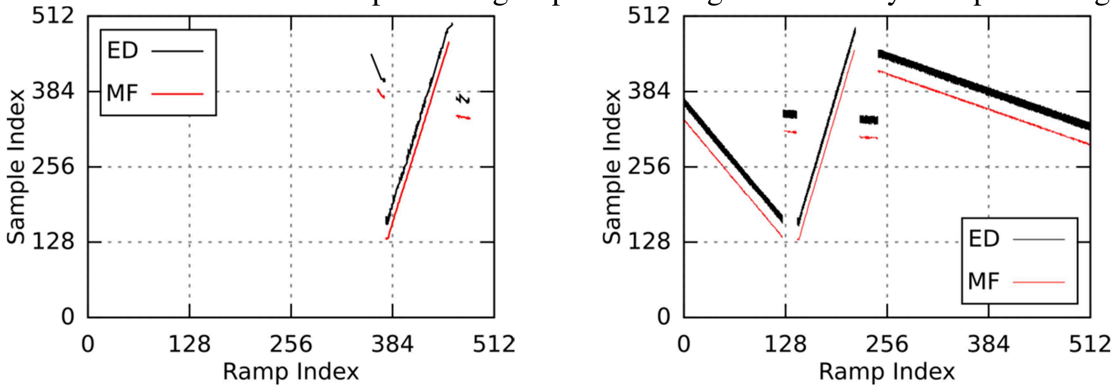

Figure 4: Detection result of a real world measurement with a weak interference signal (left) and a strong interference signal (right) using an energy detector (ED) and a single matched filter (MF). The matched filter curve has been shifted by -30 samples for improved visibility.

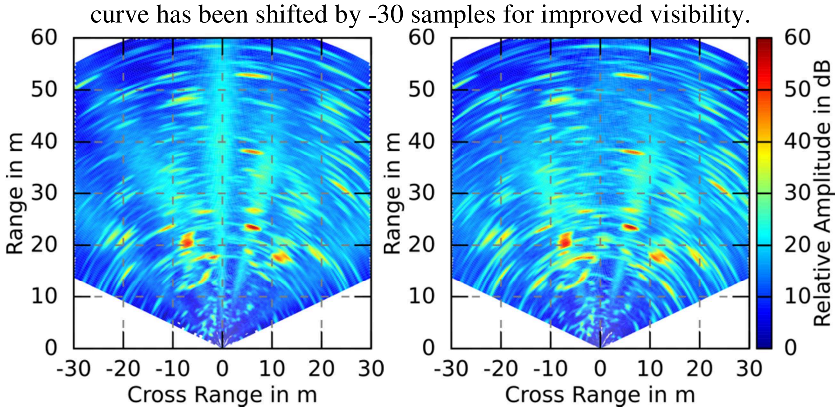

Figure 5: Processing result of the high amplitude interference scenario without interference mitigation (left) and with interference mitigation by adaptive beamforming (right).

The detection results of two different measurements with an interferer are shown in Fig. 4. It can be seen that for a high amplitude interference signal (right) the matched filter detector results a sharper line than the energy detector that has a broad band in which the interference is detected. The result of the matched filter is very close to the ideal line shape of the FMCW signal for all three different slopes present in the measurement. For a weak interference signal (Fig. 4, left) the results of matched filter and energy detector appear similar, although the energy detector has a noisier characteristic than the matched filter. From these observations one can conclude that the matched filter offers constant performance for all amplitudes, but the energy detector already fulfills the detection task well enough for some applications.

The measurement with the strong interference has been used as an example for the ABF-based mitigation method. The detection result of the matched filter detector (as in Fig. 4, right) has been used to compute the nulling coefficients. Fig. 5, shows the processed result without (left) and with (right) interference mitigation. Without mitigation, the raised noise level in the direction 0° is clearly visible. With interference mitigation, the reduced noise floor can be observed in addition to smaller targets that had been buried in the noise.

7. Conclusion and Outlook

Basic interactions of typical continuous wave radar systems have been presented in this paper. Based on these descriptions, a method for robust detection and mitigation has been developed. These algorithms have been evaluated using measurements made with an available experimental radar sensor. The applicability of the proposed methods could also be shown in combination with high resolution algorithms. Additionally, the impact of possible mutual sensor interference could be estimated with and without the proposed counter measures showing the good performance of adaptive beamforming.

References:

[1] M. Kunert, "The EU project MOSARIM: A general overview of project objectives and conducted work," in 9th European Radar Conference (EuRAD), 2012. Oct. 2012, pp. 1–5.

[2] A. G. Stove, "Linear FMCW radar techniques," Radar and Signal Processing, IEE Proceedings F, vol. 139, no. 5, pp. 343–350, Oct. 1992.

[3] M. S. Bartlett, "Smoothing periodograms from Time-Series with continuous spectra," Nature, vol. 161, no. 4096, pp. 686–687, May 1948.

[4] J. Makhoul, "Linear prediction: A tutorial review," Proceedings of the IEEE, vol. 63, no. 4, pp. 561–580, Apr. 1975.

[5] M. Goppelt, H.-L. Blöcher, and W. Menzel, "Automotive Radar – Investigation of Mutual Interference Mechanisms," Advances in Radio Science, vol. 8, pp. 55–60, 2010.

[6] D. Oprisan and H. Rohling, "Analysis of Mutual Interference Between Automotive Radar Systems," in 6th International Radar Symposium (IRS), 2005, 2005, pp. 83–90.

[7] G. M. Brooker, "Mutual Interference of Millimeter-Wave Radar Systems," IEEE Transactions on Electromagnetic Compatibility, vol. 49, no. 1, pp. 170–181, Feb. 2007.

[8] C. Fischer, M. Barjenbruch, H.-L. Bloecher, and W. Menzel, "Detection of Pedestrians in Road Environments with Mutual Interference," in 14th International Radar Symposium (IRS), 2013, Jun. 2013, pp. 746–751.

[9] M. Goppelt, H.-L. Blöcher, and W. Menzel, "Analytical investigation of mutual interference between automotive FMCW radar sensors," in 6th German Microwave Conference, Mar. 2011, pp. 312–315.

[10] H. Winner, S. Hakuli, and G. Wolf, Eds., Handbuch Fahrerassistenzsysteme: Grundlagen, Komponenten und Systeme für aktive Sicherheit und Komfort, ser. ATZ/MTZ-Fachbuch. Vieweg+Teubner, Jul. 2009.

[11] H. Rohling, "Radar CFAR Thresholding in Clutter and Multiple Target Situations," IEEE Transactions on Aerospace and Electronic Systems, vol. AES-19, no. 4, pp. 608–621, 1983.

[12] B. E. Tullsson, "Topics in FMCW radar disturbance suppression," in Radar 97 (Conf. Publ. No. 449). IET, Oct. 1997, pp. 1–5.

[13] W. F. Gabriel, "Using spectral estimation techniques in adaptive processing antenna systems," IEEE Transactions on Antennas and Propagation, vol. 34, no. 3, pp. 291–300, Mar. 1986.

[14] B. D. Carlson, "Covariance matrix estimation errors and diagonal loading in adaptive arrays," IEEE Transactions on Aerospace and Electronic Systems, vol. 24, no. 4, pp. 397–401, Jul. 1988.